INDONESIAN JOURNAL ON GEOSCIENCE
Geological Agency
Ministry of Energy and Mineral Resources

Journal homepage: http://ijog.geologi.esdm.go.id
ISSN 2355-9314, e-ISSN 2355-9306

Application of the Simple Multi-Attribute Rating Technique (SMART) for Selecting Compatible Earthquake Time Series in Liquefaction Analysis Support: Case Study in Serpong, Tangerang, Indonesia

Akhmad Muktaf Haifani[1,2,*], Topan Setiadipura[2], and Widjojo A. Prakoso[1]

[1]Faculty of Engineering, Department of Civil Engineering, University Indonesia, Depok, West Java, Indonesia
[2] Centre for Research of Nuclear Reactor Technology
National Research and Innovation Agency, Serpong, Indonesia

[*]Corresponding author: akhm020@brin.go.id
Manuscript received: January, 11, 2025; revised: July, 30, 2025;
approved: November, 25, 2025; available online: March, 17, 2026

Abstract - The earthquake hazard must be mitigated at the prospective nuclear power plant site in Serpong, Tangerang, to avoid damage to the nuclear installation infrastructure, especially the possibility of liquefaction. This study combines Probabilistic Seismic Hazard Analysis (PSHA) with Ground Motion Prediction Equation (GMPE) (Abrahamson, 2014), which is used as a probabilistic prediction model. This is to estimate spectral accelerations and Peak Ground Acceleration (PGA) based on earthquake magnitude, distance, and site characteristics. Calculations were carried out using OpenQuake for PHA calculation and Seismomatch for spectra matching analysis, which produced the deaggregation results used to define the target spectrum. Representative time histories were chosen using the SMART technique, which uses ranking and weighting to assure compliance with deaggregated magnitude-distance situations, then refined using spectral matching of 90 records while keeping nonstationary properties. Both shallow crustal and subduction events have a substantial impact on seismic demand, with the 2011 Tohoku earthquake (Mw 9.0, depth 29 km, distance 245.9 km, PGA 0.26 g) appearing as the most compatible scenario and primary contributor to possible site risks. The suggested paradigm provides a realistic solution to site-specific ground motion selection and liquefaction risk assessment, hence promoting nuclear safety and seismic resilience in tectonically active regions.

Keywords: time series, spectra matching, liquefaction, magnitude, SMART, period, distance, ranking, weighting

How to cite this article:
Haifani, A.M., Setiadipura, T., and Prakoso, W.A., 2026. Application of the Simple Multi-Attribute Rating Technique (SMART) for Selecting Compatible Earthquake Time Series in Liquefaction Analysis Support: Case Study in Serpong, Tangerang, Indonesia. *Indonesian Journal on Geoscience*, 13 (1), p.57-76. DOI: 10.17014/ijog.13.1.57-76

Introduction

The evaluation of earthquake acceleration levels at the prospective Nuclear Power Plant (NPP) locations is a critical step in understanding and mitigating the risk of liquefaction. Liquefaction is a phenomenon where saturated soil loses its strength due to seismic shaking, poses a severe threat to the stability and safety of NPP structures. Surface acceleration, as the primary trigger of liquefaction episodes, requires precise analysis to predict and to manage these hazards effectively. For example, Mase *et al.* (2022) analyzed the liquefaction potential caused by the Kobe earthquake at the Izumio site, demonstrating the importance of surface shock recordings in understanding liquefaction behaviour. Similarly, the 2009 Padang earthquake (Mw of 7.6) caused widespread destruction, fatalities,

and evidence of liquefaction, underlining the critical need for robust liquefaction risk assessments (Mase *et al.*, 2022; Yassin *et al.*, 2022).

In the seismic hazard design of nuclear power plants (NPPs), a probabilistic seismic hazard analysis (PSHA) approach is commonly used. This method integrates information from multiple potential earthquake sources to estimate ground motion parameters associated with specific return periods. The analysis involves calculating the probability that a ground motion parameter X will exceed a certain threshold x^*, for a given earthquake scenario at a particular source location. This probability is then multiplied by the occurrence rate of such an earthquake. The results from all scenarios are aggregated using the total probability theorem, typically expressed in a formal summation or integral equation (EERI, 1989).

$$P(X \geq x*) = \sum_{i=1}^{Ns} \int_{m0}^{M} \int_{r0}^{R} P[X > x* | m,r] f_{Mi}(m) f_{Ri}(r) dm dr \quad .....(1)$$

Where:

P(X≥x^* |m,r) is the total probability of the earthquake with magnitude and

r distance exceeding the specific x value,

i range from 1 to the total number of earthquake sources,

VI is the average rate of earthquake incidence for magnitude M of source I,

P(X>x^* |m,r) is the probability that earthquakes with magnitude M and

distance R will exceed the level ground motion level x* because of the aleatory variability inserted through Sigma in GMPE relationships.

The f_Mi (m) and f_Ri (r) are functions of density probability to magnitude and distance, respectively.

PSHA deaggregation is particularly valuable as it identifies dominant earthquake scenarios based on magnitude (M), distance (R), and geographic coordinates (Bazzurro and Cornell, 1999; McGuire *et al.*, 2005). These insights are critical for site-specific seismic hazard evaluations (Barani *et al.*, 2022; Haifani and Siwhan, 2022). However, despite its utility, PSHA faces significant challenges in accurately capturing the heterogeneity of seismic hazards, particularly in tectonically complex regions.

The key issues in seismic hazard analysis are:

1. The of stationarity in earthquake event ground motion characteristics. Stationarity in this context refers to the idea that both the temporal occurrence of earthquakes and the statistical behaviour of ground motion parameters remain constant over time, such as the use of stationary Poisson processes to model earthquake recurrence and ground motion prediction techniques that ignore regional or temporal variations. In tectonically active and structurally complex places, these assumptions may not adequately describe the dynamic character of seismic processes, thereby leading to underestimating or overestimation of hazard levels.
2. Relying on simple modelling assumptions that ignore the complexities of seismic hazards. Simplified techniques frequently assume spatial consistency in source and site parameters, or they utilize averaged values which might fail to capture the true heterogeneity in ground motion intensity and distribution.
3. The heterogeneity of seismic hazard characteristics, including spatial and temporal variability in seismic source mechanisms (*e.g.* strike-slip, thrust, or normal faulting), rupture processes, fault geometry, stress drop, ground motion attenuation, and site-specific effects such as basin amplification, soil nonlinearity, and topographic influences. Ignoring such heterogeneity may jeopardize the validity of seismic hazard assessments (Drouet *et al.*, 2017; McGuire, 2016; McGuire *et al.*, 2002; Silva and Derras, 2019).

Although deterministic approaches—such as direct distance estimation or the use of attenuation functions like Kanai's—may offer more specific alternatives, they are not applied in this study. Instead, these references are included to emphasize the importance of addressing distance-related

uncertainty within the broader probabilistic framework adopted here. It should also be noted that any apparent amplification of ground motion at greater distances is not due to distance alone, but is often associated with site class effects, such as basin resonance or nonlinear soil behaviour (Pitarka *et al.*, 2020; Stewart *et al.*, 2014). Additionally, ensuring statistical reliability in site amplification analysis requires at least eleven time series for each target spectrum (Zimmerman *et al.*, 2017).

Dynamic site response analysis requires time history recordings that are compatible with the MCEr-targeted response spectrum and 5 % damping mandated by seismic design standards (SNI 1726, 2020). However, a thorough evaluation of liquefaction hazards necessitates the inclusion of critical geotechnical factors. These include the average shear wave velocity in the upper 30 m (Vs_{30}), where values below 250 m/s are generally associated with highly liquefiable soils (Bommer and Acevedo, 2004; Goulet *et al.*, 2021), soil porosity and density which influence the generation of excess pore pressure and soil classifications such as loose sands or saturated silts, known to amplify liquefaction potential.

A pore pressure ratio of 0.9 is commonly acknowledged as a key threshold marking the commencement of complete liquefaction (McGuire, 2016; Wirth *et al.*, 2019). Limitations in ground motion selection, such as the simplified point-source representation in seismic deaggregation (Pitarka *et al.*, 2020; Zafarani *et al.*, 2018) and assumptions of ground motion stationarity (Drouet *et al.*, 2017; McGuire, 2016; Silva and Derras, 2019), may obscure site-specific vulnerabilities. Thus, effective liquefaction hazard categorization must consider both spectral compatibility and measurable site-specific indications.

Recent research has focused on addressing these constraints and has shown sophisticated techniques to improve seismic time series selection. Techniques such as wavelet-based spectral matching(Al Atik and Abrahamson, 2010) and genetic algorithms (Mergos and Sextos, 2019) offer promising approaches, but often demand significant computational resources. Researchers have classified seismic events based on hazard contributions, demonstrating the complexity of practical application, particularly in data-scarce regions (Hu *et al.*, 2022; Spassiani *et al.*, 2023). These challenges highlight the urgent need for innovative, efficient, and site-specific methodologies. Advances in liquefaction potential analysis have improved correlations between ground motion parameters and soil response (Bray, 2006).

Furthermore, region-specific research has highlighted the importance of adding local geological and geotechnical variables to increase hazard prediction accuracy (Idriss, 2008). In line with this, the theoretical underpinning of site response analysis is based on wave propagation concepts in layered media and the stress-strain behaviour of saturated soils under cyclic loading (Kramer, 2020). Site-specific regulations for nuclear power plants (NPPs) require in-situ measurements of shear wave velocity (Vs_{30}), standard penetration test (SPT) values, and historical seismicity data to validate their concepts. Multi-Attribute Rating Technique (SMART) provides a structured framework for evaluating seismic time histories based on key attributes such as magnitude, epicentral distance, PGA, and depth. This ensures the selected ground motions, and are not only spectrum-compatible but also reflect local site characteristics enhancing the robustness of liquefaction hazard simulations for NPP development.

Data Collection of Time Series

The selection of earthquake time series is critical for researching the behaviour of potentially liquefaction-prone soils and evaluating the performance of building foundations in such settings. These earthquake features can also help anticipate future seismic events, and build effective mitigation techniques. However, data processing presents challenges because not all earthquakes that cause liquefaction and seismic data relevant to liquefaction events can be used in the analysis. In this work, data of time series were used from the Strong Motion Virtual Data Centre (https://www.strongmotioncenter. org/vdc/scripts/earthquakes.plx) that are selected based on source distance,

magnitude, and soil types related with liquefaction situations, notably sandy soils. Primary geotechnical data, such as Standard Penetration Test (SPT), Cone Penetration Test (CPT), and shear wave velocity (Vs) profiles have been added to reinforce the analysis site-specific validity, according to the Serpong area site investigation completed by BATAN (2016). These data provide a more precise depiction of the local subsurface conditions and help the selection of suitable ground motions using the SMART approach. The deaggregation curve is also used to estimate the distance and magnitude of the dominant earthquake source, which enables the selection of representative time series for both near- and far-field scenarios. By integrating both secondary and validated primary data, the chosen ground motion set reflects a more realistic scenario of seismic excitation and liquefaction potential.

Studied Site

This study focuses on the Serpong Subdistrict in South Tangerang City, Banten Province (6° 21′ 26″S, 106° 39′ 37″E), located in the western area of Java Island. The figure depicts the spatial distribution of significant earthquake sources across the western part of Java and surrounding regions, encompassing the Sumatra and Java subduction zones as well as active faults such as Lembang, Cimandiri, and Baribis, within a 250 km and 500 km radius of Jakarta as a reference for the studied site. It integrates key seismological parameters such as earthquake depth, moment magnitude (Mw), and source mechanism (*i.e.*, shallow subduction or deep), as shown in Figure 1.

The site was chosen for its potential as a location for small modular reactors (SMRs) and its

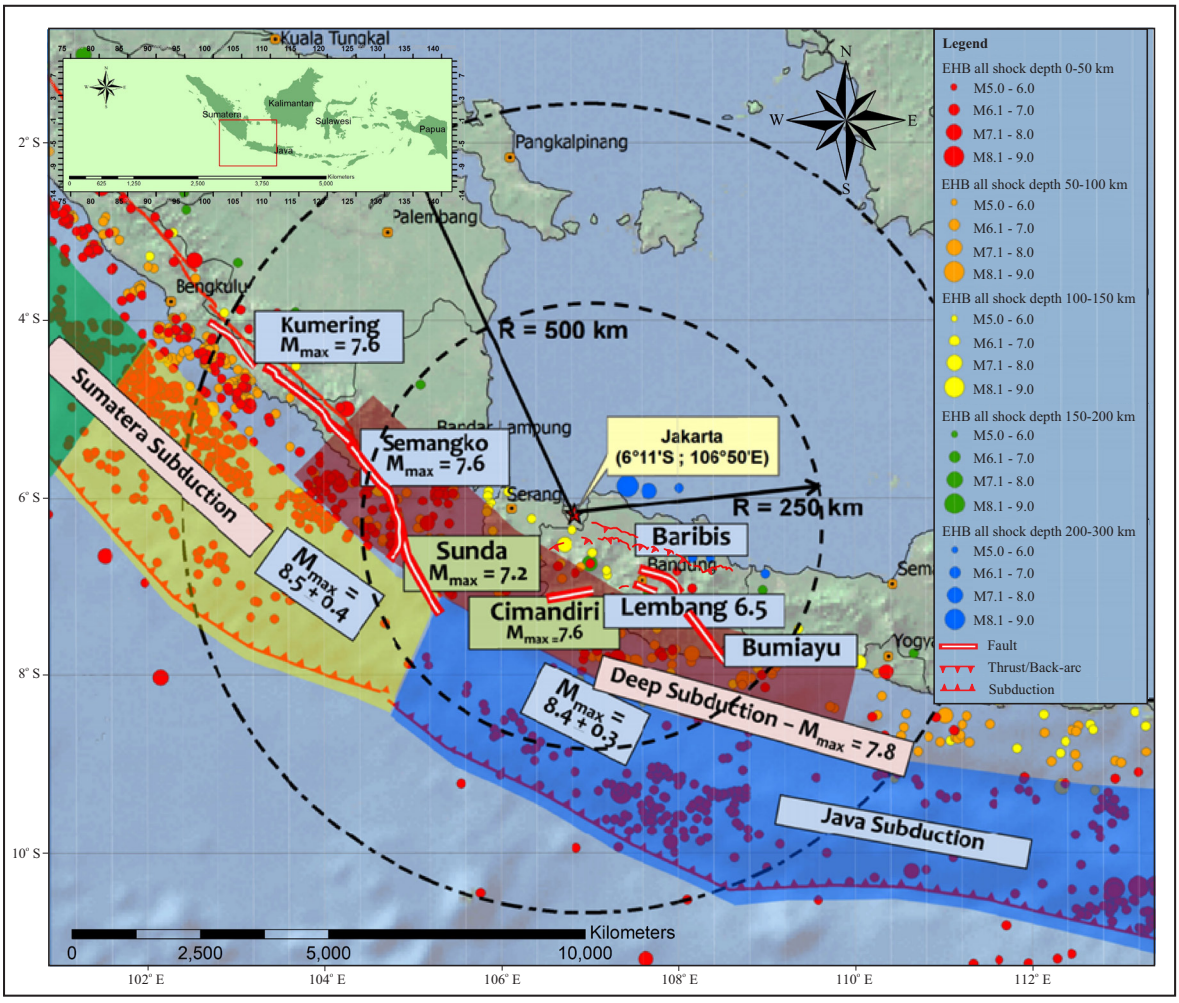

Figure 1. Earthquake source zone in the western part of Java (Irsyam et al., 2015).

proximity to known active faults. BATAN (2016) provides primary geotechnical data, including SPT, CPT, and Vs profiles, which shed light on subsurface stratigraphy and soil attributes. Geological mapping reveals young sedimentary deposits with sandy-silty layers ripe for liquefaction (Figure 2).

Methodology

Deaggregation

The deaggregation methodology used in this study adheres to the framework established by Pagani *et al.* (2014), which allows for the determination of the contribution of various earthquake scenarios—defined by magnitude and distance—to a specific ground motion level exceedance. The research was carried out on a dataset acquired from PSHA results at the planned site in Serpong, Indonesia. The PSHA deaggregation outputs provide the major input data, which include moment magnitude (Mw), projected surface rupture distance (rjb), longitude, latitude, and Tectonic Regime Type (TRT). A customized MATLAB programme was used to construct the site-specific deaggregation histogram. This programme uses hazard curves and conditional probabilities to generate joint magnitude and distance distributions that contribute to exceeding the ground motion level X at return period T. The theoretical framework is built on conditional probability functions:

$$P(X > x|T, M, r_{jb}) = 1 - \prod_{\lambda}\prod_{\Phi}\prod_{TRT}\prod_{\varepsilon}(1 - P(X > x|T, m)) \quad .....(2)$$

Where:

λ and Φ represent the spatial location (longitude and latitude),

TRT the tectonic regime, and

ε the ground motion variability.

This approach enables identification of dominant scenarios contributing to site hazard. The use of a

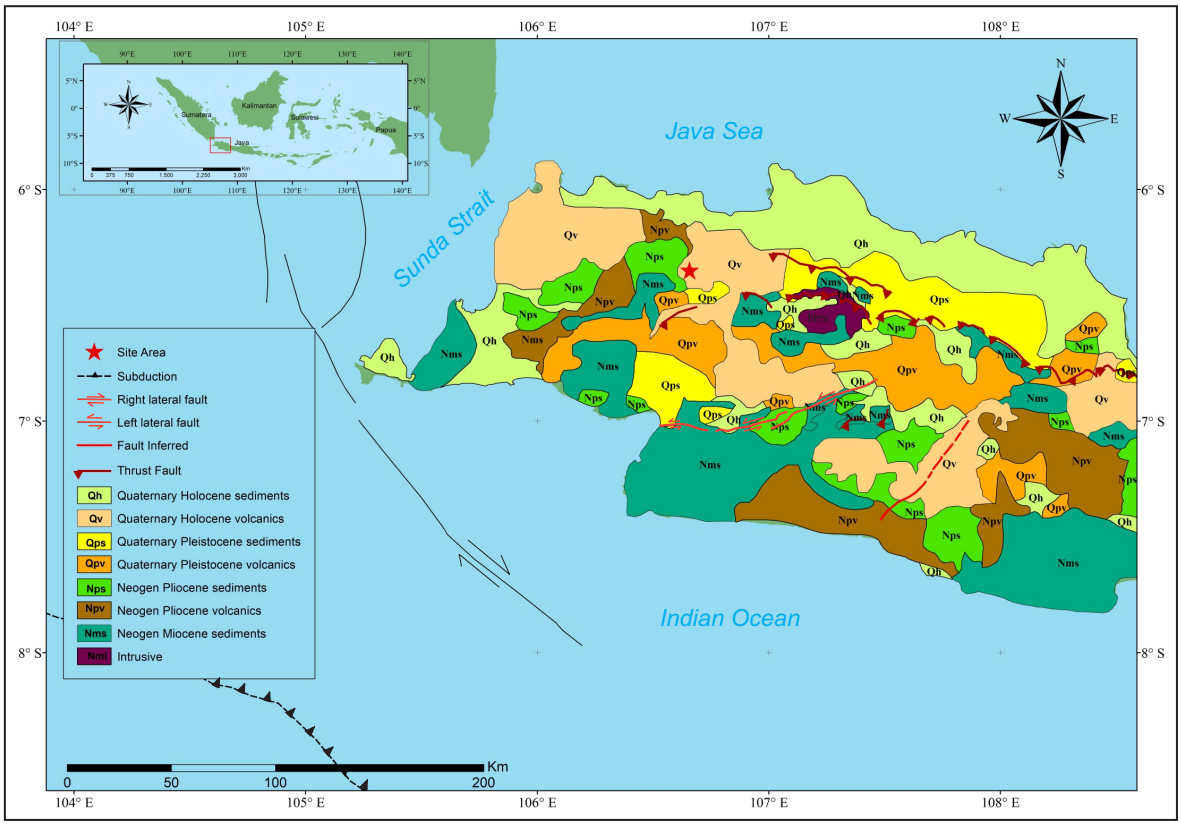

Figure 2. Simplified geological map of West Java (https://geologi.esdm.go.id/geomap, Aribowo et al., 2022, Damanik *et al.*,2021, Supendi *et al.*,2025).

histogram allows visualization of the probabilistic distribution and highlights the controlling magnitude–distance pairs. Data acquisition and hazard modelling follow Indonesian guidelines and are based on sources such as BATAN (2016), with additional processing through MATLAB scripting.

Spectral Matching

The spectral matching procedure alters ground motion data to match a target response spectrum determined from site-specific Probabilistic Seismic Hazard Analysis (PSHA). This guarantees that the selected accelerograms appropriately depict the seismic requirements at the studied location (Bani-Hani and M.A.I., 2017; Cotton *et al.*, 2006). Steps to conduct spectra matching analysis:

1. Target Spectrum Definition

The target response spectrum is defined based on PSHA results. It combines site-specific seismic factors, such as attenuation relationships and deaggregation data. This spectrum is used as a reference for calibrating the selected ground movements.

2. Selection of Ground Motion Records

Ground motion records are chosen from a database using peak ground acceleration (PGA, g), moment magnitude (Mw), and source distance (km). To determine compatibility, the response spectrum from each record is compared to the target spectrum. Records with a large frequency range are preferred to reflect realistic earthquake conditions (Irfan *et al.*, 2012).

3. Time-Domain Spectral Matching

The selected records are adjusted with the Lilhanand Algorithm (Lilhanand and Tseng, 1987; Lilhanand and Tseng, 1988) and the wavelet-based approach proposed by Al Atik and Abrahamson (2010).

These change the amplitude and phase of each accelerogram in order to better align its spectral content with the target spectrum while maintaining physical realism. It consists of the response impulse and the response function in the reverse order as stated below:

$$\alpha i(t) = \frac{\omega i}{\sqrt{1-\beta i^2}} \exp\left(-\omega i \beta i (ti - t)\right) [2\beta i^2 - 1) \sin(\omega' i (ti - t) - 2\beta i \sqrt{1-\beta i^2}\, cos\ \omega' i (ti - t))] \quad \text{.....(3)}$$

Where:

ti is the time of the peak response of the *i th* oscillator under the action of the *i th* wavelet

ωi is the circular frequency of *i th* wavelet,

βi damping level of *i th* oscillator, and

$\omega' i$ is the damped circular frequency $\omega' i = \omega i \sqrt{1 - \beta i^2}$.

Using a corrected tapered cosine wavelet, the wavelet must be updated to guarantee a zero final displacement (Abrahamson, 1992).

$$\Delta ti = \frac{\tan^{-1}\left[\frac{\sqrt{1-\beta i}}{\beta i}\right]}{\omega' i} \quad \text{.....(4)}$$

It is important to choose the subject of frequency dependence, denoted as ωi, carefully. This ensures that both the modified wavelet and the reference time series have a consistent duration at frequency ωi. In other words, if the reference time series is short at a specific frequency, then ωi should be selected in such a way that the adjustment function at that frequency will also be short (Dombi *et al.*, 2023).

4. Frequency-Dependent Adjustment

To maintain time consistency across frequency bands, a trilinear model is used:

$$\omega i = z1 \quad \text{if for fi} < f1 \quad \text{.....(5)}$$

$$\omega i = z1 + (z2 - z1) + \frac{(f - f1)}{(f2 - f1)}$$

if for f1<fi<f2

$$\omega i = z3 \quad \text{if for f1>f2}$$

Where:

f1, f2, zl, and

z2 are constant and

fi is frequency of *i th* wavelet in Hz;
constant of f1 = 1 Hz, f2 = 4Hz, z1 = 1.25 and z2 = 0.25.

To eliminate residual displacement, the adjustments use the corrected tapered cosine as follows:

$$\alpha i(t) = \cos[\omega' i(t - ti\Delta ti)]\exp[-|t - tj + \Delta t|\,\omega i + [c1(t - ti + \Delta ti) + c2]\exp[-|t - ti + \Delta ti|5\omega i] \quad \text{.....(6)}$$

where consists c1 and c2 depend on site-specific parameters, and Δt ensures consistent time duration.

5. Validation of Matched Records

Accelerograms are validated by comparing their response spectra to the target spectrum. Records with low amplitude and frequency deviations are selected due to their consistency with site-specific deaggregation results.

6. Iterative Refinement

The matching process is iterative, with amplitude and phase refined until the accelerogram spectrum roughly matches the target spectrum throughout all frequency bands. The emphasis is on high-frequency components, which play an important role in nonlinear structural response and energy dissipation during significant ground shaking.

7. Final Output

The output comprises of spectrally matched accelerograms that depict the site's seismic danger. These are employed in additional structural and geotechnical assessments, especially nonlinear dynamic and liquefaction models.

Earthquake Frequency Distribution

To analyze the distribution of seismic events and ground motion intensities, the earthquake frequency distribution is used. This method divides data into intervals and provides insights into the frequency of events within certain ranges. The statistical technique employed allows for a deeper understanding of seismic activity at a given site by organizing the data into frequency distributions (Dheeraj Vaidya, 2023; Dombi *et al.*, 2023; Liu *et al.*, 2023; Miller, 2015). These distributions create a framework for evaluating ground motion characteristics and understanding the probabilistic seismic hazard.

To classify the distribution of ground motion data that has undergone spectral matching, class intervals are developed. The frequency distribution was determined using the steps adapted from Gonick (1993).

First, the data class width was calculated based on the range of ground motion values:

$$Data\ class = Maximum\ value - Minimum\ value \quad \text{.....(7)}$$

Next, the number of observation classes was estimated using Sturges' formula.

$$Number\ of\ class = 1 + 3.2 \log (Number\ of\ Data\ Set) \quad \text{.....(8)}$$

The relative frequency was then derived as:

$$Relative\ Frequency = \frac{Absolute\ Frequency}{Number\ of\ Data\ Set} \quad \text{.....(9)}$$

This approach organizes the distribution of ground motion data in a clear and statistically structured format, facilitating subsequent analysis and interpretation.

Artificial Weighting for Time Series

The weighting factor refers to the importance assigned to each item in a data set to determine whether it is considered primary or secondary within the group. This study describes the weighted average of matched time series data that is most likely to contribute to hazard assessment based on its characteristics. To account for the varying significance of each seismic event in hazard estimation, an artificial weighting mechanism is applied to the time series data. This method employs the Simple Multi-Attribute Rating Technique (SMART) to assign weights to each ground data point based on four key earthquake characteristics: epicentre, Peak Ground

Acceleration (PGA), distance, and magnitude. Weights can be calculated using the following formula (Mardani *et al.*, 2015), which follow the stages for performing a SMART analysis (Equations 9 and 10).

$$w_i = \frac{P_i}{\sum_i^n P_i} \quad \text{.....(10)}$$

$$P_i = x_1 + x_2 + x_3 + \cdots x_n \quad \text{.....(11)}$$

Where:

w_i= weighted value in percent for each criterion,

P_i = score of each time series to be weighted.

In this study successively the weight values for x_1= distance, x_2= magnitude, x_3= PGA, and x_4= source depth.

The SMART analysis assigns weights to each attribute based on its contribution to the overall seismic hazard. By assigning more weight to recordings from closer distances, larger magnitudes, or stronger ground motions, the model ensures that more significant events contribute more significantly to seismic hazard assessment.

Result

Seismic Deaggregation

Probabilistic seismic hazard analysis produces both a hazard curve and a response curve using bedrock data. The next step is to conduct a deaggregation analysis to identify which earthquake occurrences contribute most significantly to the overall risk, based on their magnitude (M) and hypocentre distance (R). The hypocentre distance indicates the latitude and longitude of the earthquake source. The analysis calculates the weighted average values of R and M for all sources contributing to the hazard at each kilometer location, reporting these as mean distances and average magnitudes. At each specified location, the most prominent hazard deaggregation is represented by a specific pair of distance and magnitude (R, M).

Figure 3a illustrates the deaggregation computation centred at a latitude of -6.357 S and a longitude of 108.66 E. In this experiment, a distance width of 30 km (R) and a magnitude bin of 0.5 were selected (Figure 3b). The highest calculated source for shallow crustal earthquakes in the researched area ranges from 10 to 30 km. In a subduction zone, the maximum distance to

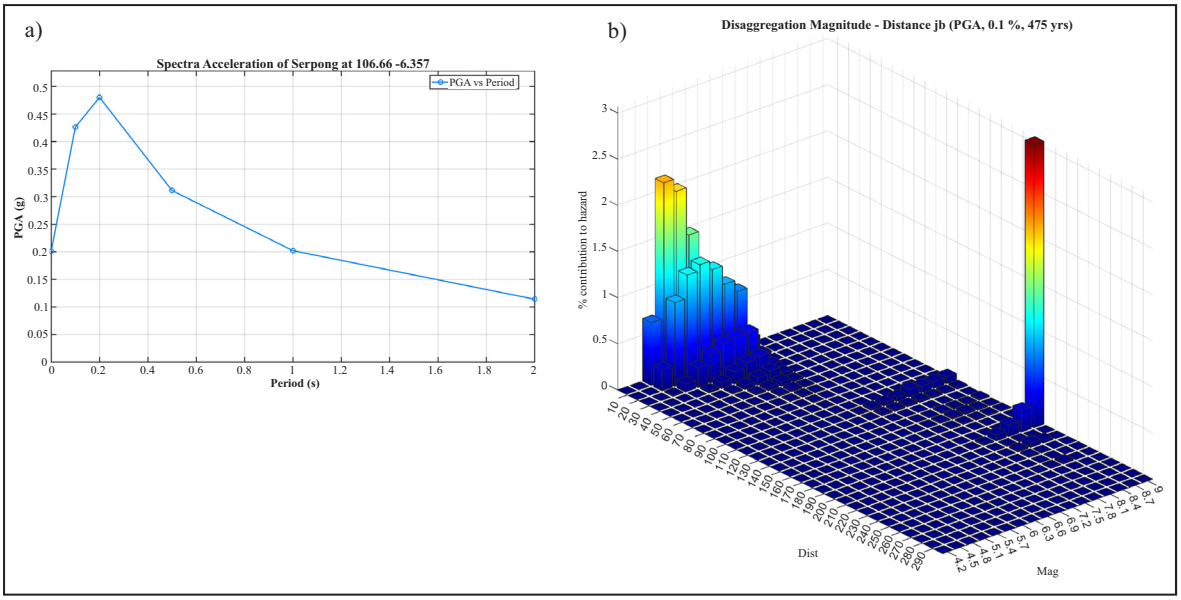

Figure 3: PSHA calculation results: a) Hazard curve for the 500-year return period (BAPETEN, 2013) ; b) Deaggregation histogram for the Serpong area with the highest hazard contribution to the earthquake source at 210 km and 9 Mw.

an active earthquake source is between 130 and 210 km.

Spectra Matching of Seismic Wave

The findings from the PSHA calculation were used to determine the initial ground acceleration, which corresponds to the deaggregated earthquake values from the proposed NPP site in Serpong. The earthquake spectrum data were then adjusted to align closely with the spectral response of the specified target. Figure 2 illustrates the results of this spectrum matching as a time series of acceleration, velocity, and displacement at T= 0 seconds. The target spectral response is defined with a 5 % damping level, a 500-year return period, and a 10 % probability over fifty years, leading to a change in the time series pattern compared to the original data.

The time series was selected based on technical assessments of the suitability of the earthquake event for the intended site, as well as evaluations of the liquefaction-producing seismic event. The study utilizes the following variables: Distance and magnitude from the earthquake source (Bardet and Tobita, 1992), determined from the results of the deaggregation curve (distance: 210 km; Mw: 9), frequency range of 0.5 to 10 Hz, earthquake amplitude between 0.05 and 1 g, earthquake duration ranging from 10 to 60 seconds, Mw from 5 to 9, type of sandy soil and time series data recording local earthquakes, specifically the Lebak earthquake of 5.9 Mw that occurred on January 23, 2018. Although the disaggregation analysis indicates a dominant scenario of a subduction event with Mw 5 and a source-to-site distance of approximately 210 km, the Lebak earthquake (Mw 5.9, 2018) was selected for time series analysis due to its availability and suitable frequency and amplitude characteristics. It is acknowledged that the Lebak event does not match the dominant hazard scenario in terms of depth or distance, and the results obtained from this time history are therefore intended for comparative purposes rather than direct representation of the deaggregated hazard.

A total of 175 local and global earthquake data points were evaluated based on the results of the data selection technique. For the analysis, ninety distinct earthquake data sets were chosen to represent individual seismic events. This approach enables an objective study that accurately reflects the earthquake source characteristics examined in the site reaction analysis.

The Tohoku earthquake on March 11, 2011, formed a part of the time series chosen to represent the source of the earthquake, because it shared characteristics with the deaggregation curve values (Figure 4). The SEISMOMATCH 2018 programme is used to process spectral matching data. During the spectral matching analysis of recordings, wavelet adjustment in the time domain was performed. Time series with a scale factor of 0.52 and a tolerance of 0.4, a maximum period limit value of (0.05) seconds, and a maximum period limit value of 4 seconds are chosen. The investigation provided a reasonable scaling with an average misfit of 3.9 % and a maximum misfit of 38.6 % after the required six iterations.

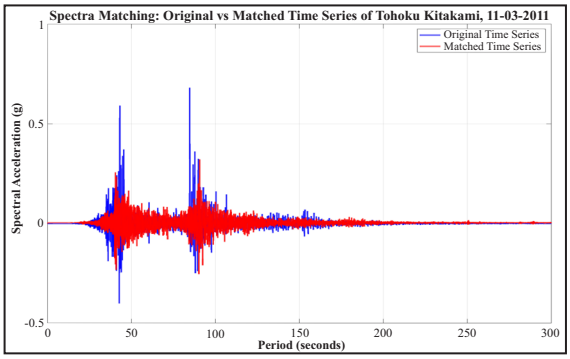

Figure 4 Comparing Tohoku Sendai Original to Matched Time history for the Serpong area.

Frequency Distribution of Data

PGA variation was analyzed using ninety matched time series that represent the target bedrock ground motion spectrum. The deaggregation curve was analyzed using distance and magnitude parameters (magnitude 9 and distance 210 km) to filter the time series. Additionally, the PGA earthquake parameters and source depth, as pre-

sented in Tables 1-4, indicate that the time series are compatible with the ground motion designs.

The “class” column shows the PGA intervals. The “PGA” column lists their ranges in "g". “Absolute F” is the count of events in each interval, and “Relative F (%)” shows their proportion to the total number of observations.

For the frequency distribution, the PGA (Peak Ground Acceleration) fluctuations are classified into the following values: PGA minimum= 0.1 g, PGA maximum= 0.48 g, PGA range= 0.35 g, number of PGA classes= 8, and length of each PGA class = 0.04 g.

Among the total observations, there were thirty-eight earthquake events in class 4 with magnitudes ranging from 0.2 to 0.24 g, representing 42 % of all the recorded events (Table 1 and Figure 5). The distribution of PGA intervals is as follows: 0.1–0.14 g: eight events (8.89 %), 0.15–0.19 g: twenty-nine events (32.22 %), 0.25–0.29 g: seven events (7.78 %), 0.3–0.34 g: four events (4.44 %), 0.35–0.39 g: one event (1.11 %), 0.4–0.44 g: two events (2.22 %), 0.45–0.49 g: one event (1.11 %). Table 1 shows the distribution of PGA values across all intervals frequency distribution (R) parameter as follows: The minimum distance (Rmin) is 4 km, and the maximum distance (Rmax) is 363 km. The total range (R) is 359 km, and there are eight classes, each with a class length of 44 km.

In Class 1, which covers the distance range of 4−48 km, there were forty-nine recorded earthquakes. This class represents 54.44 % of all observations, indicating it has the highest frequency of events. Additionally, the following observations were noted as a percentage of the total events: three earthquakes occurred in the range of 49−93 km, accounting for 36.67 %, eight earthquakes were recorded between 88.8 and 131.6 km, representing 5.56 %, There was one earthquake each in the ranges of 139−183 km, 229−273 km, and 319−363 km, with each range contributing 1.11 % of the total observations (as shown in Table 2 and Figure 6).

The frequency distribution of the depth parameter is as follows: Minimum depth (Dmin): 2 km, - Maximum depth (Dmax): 113 km, Depth range (D range): 107 km, Number of depth classes: eight, Class depth length: 13 km. A total of fifty-one events of class 1 earthquakes was recorded in the depth range of 2−15 km, which accounts for 35.4 % of all observations in the most frequently

Table 1. Frequency Distribution of PGA

Class	PGA (m/s²)	F-Absolute (f)	F-Relative (%)
1	0.1-0.14	8	8.89
2	0.15-0.19	29	32.22
3	0.2-0.24	38	42.22
4	0.25-0.29	7	7.78
5	0.3-0.34	4	4.44
6	0.35-0.39	1	1.11
7	0.4-0.44	2	2.22
8	0.45-0.49	1	1.11
Total		**90**	**100.00**

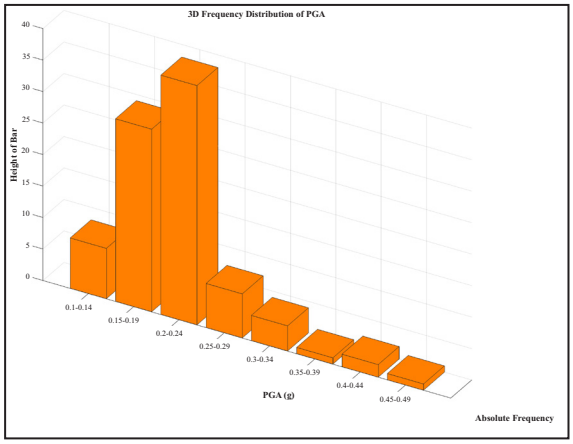

Figure 5. PGA Frequency Distribution Column.

Table 2. Frequency Distribution of Distance (R)

Class	Distance (km)	F-Absolute (f)	F Relative (%)
1	4-48	49	54.44%
2	49-93	33	36.67%
3	94-138	5	5.56%
4	139-183	1	1.11%
5	184-228	0	0.00%
6	229-273	1	1.11%
7	274-318	0	0.00%
8	319-363	1	1.11%
Total		**90**	**100.00**

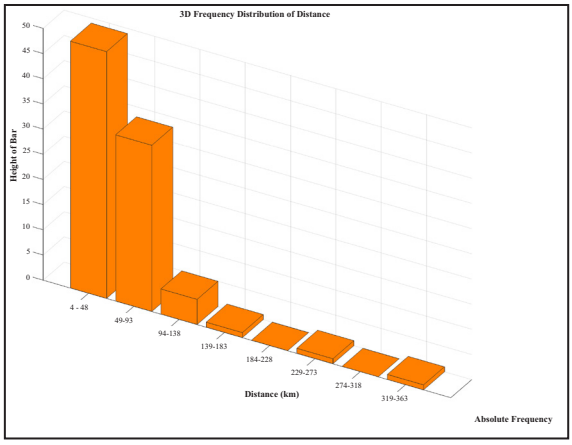

Figure 6. Distance Frequency Distribution Column.

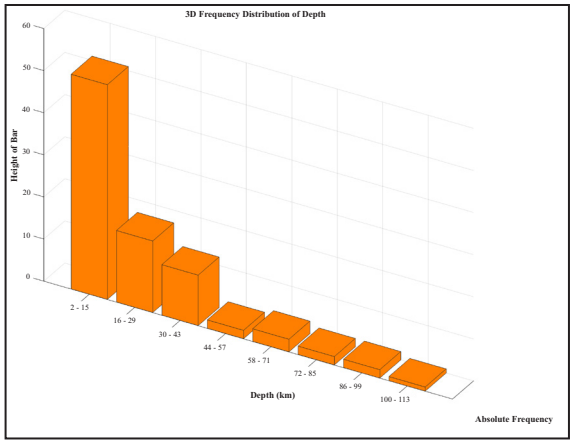

Figure 7. Depth Frequency Distribution Column.

occurring depth range. The distribution of events across different depth ranges is as follows: 16-–9 km: forty-two events (42 %), 30−43 km: twelve events (29 %), 44−57 km: two events (13.4 %), 58−71 km: three events (0.6 %), 72−85 km: two events (1.7 %), 86−99 km: two events (2.22 %), 100−113 km: two events (2.22 %) (Table 3 and Figure 7 for further details).

According to the frequency distribution of the magnitude (Mw) parameter, the minimum magnitude (Mmin) is 4.5. The range of magnitudes (M) is 4.5 with the number of classes (R) set at 8 and the class interval length set at 0.6. The most frequently occurring earthquake magnitude range is between 6.82 and 7.32, which includes twenty-four events and accounts for 26.67 % of the total observations (Figure 8). The distribution of other magnitude ranges is as follows: seventeen events (18.89 %) for the interval between 4.5 and 5, sixteen events (17.78 %) for the interval between 5.08 and 5.66, eight events (8.89 %) for the interval between 5.66 and 6, eleven events (12.22 %) for the interval between 6.24 and 6, one event (1.11 %) for the interval

Table 3. Frequency Distribution of Depth

Class	Depth (km)	F-Absolute (f)	F-Relative (%)
1	2-15	51	56.67
2	16-29	17	18.89
3	30-43	12	13.33
4	44-57	2	2.22
5	58-71	3	3.33
6	72-85	2	2.22
7	86-99	2	2.22
8	100-113	1	1.11
Total		**90**	**100.00**

Table 4. Frequency Distribution of Magnitude

Class	Mag	F-Absolute (f)	F-Relative (%)
1	4.5-5	17	18.89
2	5.08-5.58	16	17.78
3	5.66-6.16	8	8.89
4	6.24-6.74	11	12.22
5	6.82-7.32	24	26.67
6	7.4-7.9	12	13.33
7	7.98-8.48	1	1.11
8	8.56-9.06	1	1.11
Total		**90**	**100.00**

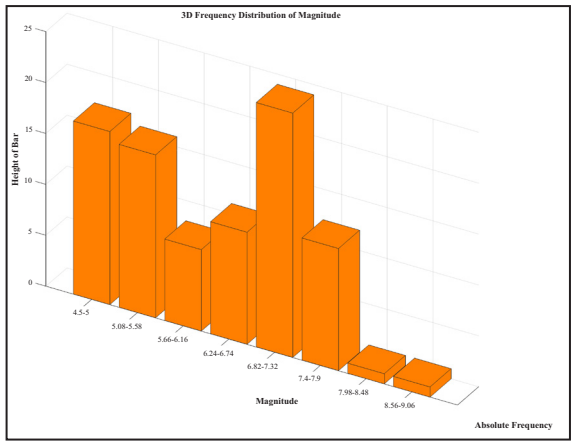

Figure 8. Magnitude Frequency Distribution Column.

between 7.98 and 8, one event (1.11 %) for the interval between 8.56 and 9. This data highlights the prevalence of a certain magnitude ranges in earthquake occurrences

To clarify the distribution of the primary parameters used in this study, histograms and heat maps were created. The histogram in Figure 9 illustrates the relationship between earthquake distance (in km) and peak ground acceleration (PGA in g), which helps to understand how both parameters influence the spectral response. Figure 10 presents a heat map showing the simultaneous distribution of earthquake magnitude and depth.

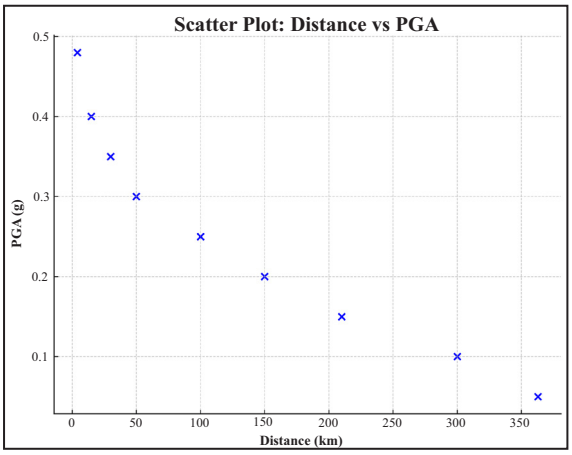

Figure 9. A scatter plot illustrating the relationship between PGA (g) and distance (km). Higher PGA values are usually generated by closer earthquakes, though anomalies can occur given other variables that influence such magnitude.

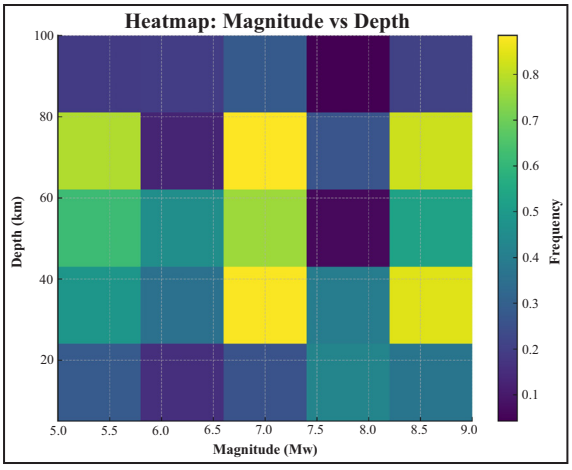

Figure 10. This heat map represents the frequency distribution of earthquakes by depth (km) and magnitude (Mw). Shallow earthquakes of moderate to high magnitude are discovered happening at higher rates.

Finally, the scatter plot in Figure 11 displays the frequency distribution of distance (R), PGA, depth (D), and magnitude (M), PGA (g), depth (km), and magnitude (Mw). These distributions show the dominant ranges for each parameter.

Weighting Factor

The table below presents the results of the deaggregation analysis, specifically the limit values used in this study. The initial weighting standard is based on the number of classes. The number of classes utilized for weighting is determined by calculating the distribution function, which considers various earthquake parameters such as distance, magnitude (with a maximum deaggregation limit of 210 km and 9 Mw), PGA (Peak Ground Acceleration), and the depth of the earthquake source (Table 5). As the class value increases, so does the weight factor. Class 8 is identified as the most significant factor, showing the greatest impact on the destruction caused by earthquakes. The factors used for selecting an appropriate time series are detailed in Table 5. Class 8 has the highest weighting factor for earthquake parameters: distances greater than 190 km, magnitudes exceeding 8.9, PGAs above 0.43, and depths of 14 km. Conversely, Class 1 earthquakes have the least impact, characterized by a distance of 70 km, a magnitude greater than 4.7, a PGA of 0.07, and a depth greater than 98 km. However, Class 1 represents the smallest scale of impact.

It should be noted that Tables 1−4 show frequency distributions calculated statistically from PGA, distance, magnitude, and depth, with classes 1−8 specified as interval ranges. Table 5 reorganizes these values into normalized impact levels using the SMART weighting scheme, with Classes 1−8 representing the least to the most critical impact rather than raw frequency intervals. Table 5 shows seismic parameters; however, site-specific elements affecting liquefaction (Vs_{30}, SPT, and CPT) were evaluated during the pre-selection of time series to ensure that ground motions relevant to liquefaction-prone circumstances were included.

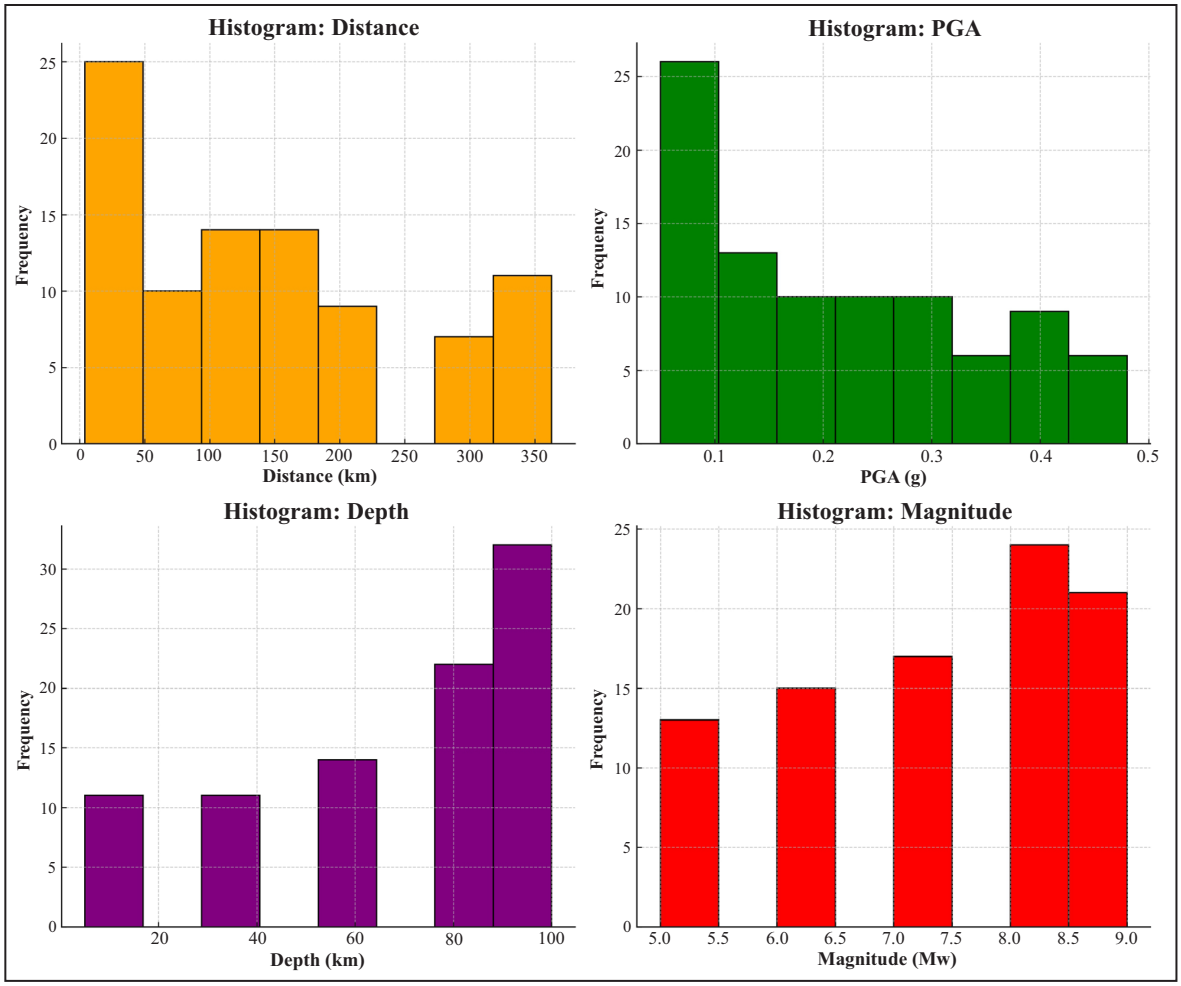

Figure 11. Histograms depicting the frequency distribution of seismic features including distance (km).

Table 5. Weighting Factors for Four Characteristics Used to Calculate The Contribution of Earthquake Sources

Class	Parameter			
	Distance (km)	Magnitude	PGA	Depth (km)
1	< 70	>4.7	<0.07	> 98
2	< 60	>5.37	>0.07	> 84
3	< 50	>5.97	>0.13	>70
4	< 40	>6.57	>0.19	>56
5	< 30	>7.17	>0.25	>70
6	< 20	>7.77	>0.31	>28
7	< 10	>8.37	>0.37	>14
8	> 190	>8.97	>0.43	<14

Table 6 presents the results of the weighting factor calculation used to identify the time series scaling results that most significantly influence potential NPP (Nuclear Power Plant) locations. This table details the findings from the assessment of ninety time series, represented by the twenty seismic events that inflicted the most damage and demonstrated the highest compatibility. The criteria examined include depth, distance, magnitude, and PGA (Peak Ground Acceleration) values. One notable event analyzed is the Tohoku earthquake, which occurred in Kitakami on March 11, 2011, at 05:46:24 UTC. The earthquake had a depth of 29 km, an epicentre radius of 245.91 km, a magnitude of 9, and a PGA score of 0.26. The evaluation based on the earthquake source distance, magnitude, PGA, and depth resulted in scores of 8, 8, 5, and 6, respectively. The total score for these four parameters is 27. The score of the Tohoku earthquake (27) accounts for 0.0174, or 1.74 % of the total score from the ninety events (1550). When the data was organized, this score indicates that the Tohoku earthquake was the event that caused the most damage, possessing

Table 6. Twenty Weighted And Scored Events with The Highest Presentation Value Out of Ninety Time Series

No	Event	Weighted Parameter				Class					Total	Percent	%
		Depth (D-km)	Dist. (R-km)	Mag	PGA	Event	R	M	PGA	D			
1	Tohoku. Japan 2011-03-11 05:46:24 UTC. Kitakami	29	245.91	9	0.26	Liquified	8	8	5	6	27	0.0174	1.7419
2	Amberley New Zealand 2016-11-13. Te Mara Farm Waiau	23	15.56	7.8	0.34	Liquified	5	6	6	7	24	0.0155	1.5484
3	Chi-Chi. Taiwan Earthquake 1999-09-20.Chiayi. Taiwan. CHY010	19	32.21	7.6	0.47	Liquified	4	5	8	7	24	0.0155	1.5484
4	Kaikoura, New Zealand 2016-11-14, Te Mara Farm Waiau GNS	10	19.18	6.5	0.24	Liquified	8	3	4	8	23	0.0148	1.4839
5	Kumamoto-shi Japan 2016-04-15. KMM006	10	5.46	7	0.23	Liquified	7	4	4	8	23	0.0148	1.4839
6	Niigata Earthquake. 16th June 1964. 040143. Niigata Prefecture	40	27.22	7.6	0.20	Liquified	5	8	4	6	23	0.0148	1.4839
7	Gazli 1976-05-17 Karakyr. Uzbekistan	15	4.01	7	0.24	Liquified	7	4	4	7	22	0.0142	1.4194
8	Imperial Valley 1979-10-15,Agraris,Mexico,Bonds Corner	10	6.39	6.5	0.21	Liquified	7	3	4	8	22	0.0142	1.4194
9	Landers 1992-06-28, Joshua Tree. CA - Fire Station	7	15.64	7.3	0.20	Not Liquified	5	5	4	8	22	0.0142	1.4194
10	Northridge 1994-01-17, Pacoima Dam. CA. 24207 (CSMIP)	17.5	5.48	6.7	0.20	Liquified	7	4	4	7	22	0.0142	1.4194
11	South West, 10 km Haast 2005-05-02, DC Workshop	13	8.16	6.2	0.22	Not Liquified	7	3	4	8	22	0.0142	1.4194
12	Superstition Hills 1987 Superstition Mtn. CA - Camera Site	9	7.50	6.5	0.19	Liquified	7	3	4	8	22	0.0142	1.4194
13	Cass 1995-11-24. Hanmer Springs. NZ - Fire Station	7	28.13	6.2	0.27	Not liquified	5	3	5	8	21	0.0135	1.3548
14	Christchurch, New Zealand 2016-02-14, Ouruhia	10	20.32	5.8	0.18	Liquified	8	2	3	8	21	0.0135	1.3548
15	Cook Strait. New Zealand 2013-07-21. UTC Ward Fire Station	14	36.20	6.5	0.34	Not Liquified	4	3	6	8	21	0.0135	1.3548
16	Eastern Honshu. Japan 2008-06-13. Furukawa	7.8	50.50	6.9	0.41	Not Liquified	2	4	7	8	21	0.0135	1.3548
17	Loma Prieta/Santa Cruz Mountains 1989-10-18, Corralitos. CA	17.5	8.90	7	0.18	Liquified	7	4	3	7	21	0.0135	1.3548
18	Cape Mendocino/Petrolia 1992-04-25, CA - Petrolia	9.6	13.76	7	0.17	Not Liquified	5	4	3	8	20	0.0129	1.2903
19	Kobe 1995-01-16. Kobe KJMA	17.9	21.10	6.9	0.20	Liquified	5	4	4	7	20	0.0129	1.2903
20	Near the Coast of Guerrero 1985-09-21. Zihuatanejo. Mexico.	30	29.88	7.6	0.22	Liquified	5	5	4	6	20	0.0129	1.2903

the highest percentage value compared to the other ninety events analyzed.

Figure 10 illustrates the response spectrum of ninety selected and scaled time series, along with the target spectrum derived from Probabilistic Seismic Hazard Assessment (PSHA) calculations. This target spectrum corresponds to a 10 % probability of exceedance over 50 years for the prospective Nuclear Power Plant (NPP) site in Serpong. The average spectrum is assumed to resemble the target spectrum to effectively evaluate the results of the spectral scaling analysis (Figure 12). To ensure the sample is representative and unbiased, ninety time-series were randomly selected from a broader subset of the population and scaled them accordingly. This approach allows us to statistically validate that the target spectrum reflects the mean spectrum of this random sample. The time series selection includes data from the Tohoku earthquake, and the resulting plot demonstrates a better alignment with both the mean and average spectra.

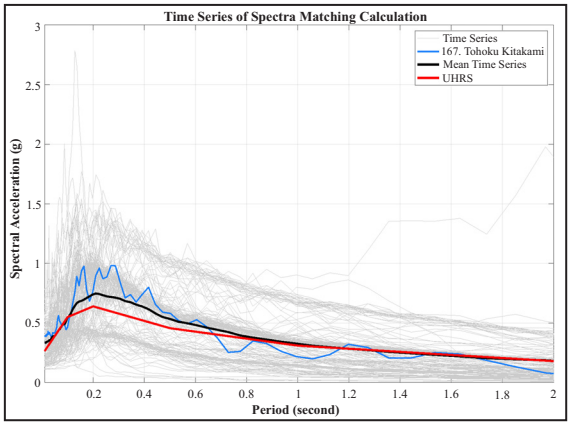

Figure 12. The geometric mean pseudo-accelerated response spectrum of ninety records with a chosen and 5 % damping scaled.

Discussion

The seismic deaggregation study results (Figure 3b) give valuable information about the primary seismic sources affecting the planned NPP site in Serpong. It shows that high-contributing earthquake scenarios are primarily formed from two types of seismic sources: subduction megathrust events, with source-to-site distances of around 190–210 km, and shallow crustal events, with distances ranging from 10–20 km. This weighting approach was based on the Simple Multi-Attribute Rating Technique (SMART), which combines these four characteristics into a single ranking framework. As a result, the Tohoku earthquake emerged as the top-ranked event, indicating the highest compatibility with the Serpong site hazard profile and exhibiting the most devastating subduction scenario. These findings support previous observations in the Indonesian region, particularly those that emphasize the dual hazard effects of regional subduction zones and local fault systems.

The distribution of earthquake data, such as average magnitude (Mw 4.25-7.25), source distance (14.89–45.35 km), depth (13–27 km), and PGA (0.18–0.24 g), illustrates both local and regional seismic activity. Hanifa *et al.* (2014) reported similar ranges in their seismic microzonation study in West Java, where shallow thrust fault earthquakes were identified as the primary drivers to near-field ground motion hazards (Hanifa *et al.*, 2014). This magnitude-distance connection demonstrates the accuracy of the earthquake scenarios chosen for seismic hazard simulation at the Serpong site.

Furthermore, an examination of the frequency distribution from ninety selected time series revealed that the majority of destructive earthquakes at the candidate site had shallow focal depths and moderate-to- large magnitude. This pattern is similar with findings from Japanese case studies such as the Niigata (1964) and Tohoku (2011) earthquakes, which showed that shallow seismic sources are more likely to generate surface ground deformation and soil liquefaction (Kagawa *et al.*, 2012; Kramer, 2020).

This finding is consistent with the ground motion patterns described by Widiyantoro who discovered that subduction earthquakes in southern Java contributes significantly to high PGA values at inland sites due to their large energy release and vast rupture (Widiyantoro *et al.*, 2022). The selection of the Tohoku earthquake as a reference spectrum is supported by strong-motion data published by the Japan Me-

teorological Agency (2011), which documented long-duration, high-amplitude shaking across a large area (JMA, 2011)

When using the Tohoku earthquake as a spectral reference, scientists used a weighting system that prioritized magnitude (Mw), PGA (g), depth (km), and source distance (km). It should be noted that Tables 1–4 show frequency distributions calculated statistically from PGA, distance, magnitude, and depth, with classes 1–8 specified as interval ranges. Table 5 reorganizes these values into normalized impact levels using the SMART weighting scheme, with Classes 1−8 representing the least to the most critical impact rather than raw frequency intervals. Table 5 shows seismic parameters; however, site-specific elements affecting liquefaction (Vs_{30}, SPT, and CPT) were evaluated during the pre-selection of time series to ensure that ground motions relevant to liquefaction-prone circumstances were included. The Tohoku event (Mw 9, PGA 0.26 g, depth 29 km, distance 245.91 km) emerged as the top-ranked scenario. This choice is congruent with the approach of Bazzurro and Cornell (2004 who argue for spectrum-compatible and hazard-consistent time histories in performance-based seismic engineering. The Amberley earthquake (Mw 7.8, PGA 0.34 g, distance 15.56 km) provided a high-fidelity temporal history for examining nonlinear site response due to its proximity and spectral richness.

The use of spectrally matched accelerograms in this work strengthens the reliability of the site response simulations. According to Abrahamson *et al.* (2008) and Hashash *et al.* (2016), time histories utilized for nonlinear dynamic analysis must keep the envelope and frequency content of the original records in order to maintain nonstationarity. The spectral matching approach used here successfully preserved these properties, as seen by time series envelope comparisons and response spectrum fidelity across the selected records.

This discussion also makes an important analytical contribution by emphasizing filtering for independent earthquake events. This method prevents artificial grouping or over-representation of repeated aftershock sequences, which can skew PGA and magnitude distributions. By concentrating on isolated main shocks, the statistical representativeness of the chosen recordings improves, increasing the reliability of deformation prediction under realistic seismic situations.

Compared to Hanifa *et al*. (2014) who explored seismic hazards in Bandung region, the current analysis provides a more comprehensive hazard profile for the Serpong location. While Hanifa's research emphasizes shallow crustal sources with thrust fault mechanisms as the primary drivers to ground motion. The data show that subduction earthquakes, particularly those from the Sunda megathrust, have a substantial influence on the PGA and response spectrum at Serpong. This disparity emphasizes the need of multiscenario deaggregation analysis in capturing both local and regional hazard factors.

Furthermore, this study focuses on spectrum-compatible and envelope-preserving time histories goes beyond the methodologies used by Bazzurro and Cornell (2004) who stressed compatibility, but did not account for long-duration waveform impacts (Bazzuro and Cornel, 2004) as seen in the Tohoku event. In contrast, the analysis reveals that the selected and matched accelerograms preserve crucial nonstationary features, indicating that they can be used in nonlinear deformation modelling. These refinements support the methodological benefit of integrating deterministic and probabilistic selection approaches, particularly for critical facilities like nuclear power plants.

Conclusion

This paper describes a comprehensive method for choosing representative ground motion data to evaluate seismic hazards and liquefaction potential at the planned nuclear power plant (NPP) location in Serpong, Indonesia. The results of seismic deaggregation and spectrum match-

ing show that both shallow crustal earthquakes and subduction megathrust events have a major impact on seismic demand at the Serpong area. Notably, the 2011 Tohoku earthquake with its extended duration and high PGA, was chosen as the most likely scenario due to its spectral compatibility and damage potential.

Using the SMART technique for time history selection, the study successfully blends site-specific seismic properties into ninety independent earthquake scenarios. These time series preserve nonstationary properties that are critical for assessing nonlinear site response and liquefaction triggering. The data show that ground motions with PGA ranging from 0.18 to 0.24 g, depths of 13 to 27 km, and magnitudes of 4.7 to 7.1 are most likely to occur and cause structural damage or soil failure at the location.

This work helps increase the dependability of ground motion selection in the context of nuclear safety and hazard assessment. It contributes to the broader goal of incorporating probabilistic hazard evaluations into nuclear siting and design techniques, particularly in seismically active regions such as Java. The technique and findings reported here can be used as a practical framework to improve seismic resilience and guide future liquefaction risk assessments at additional important infrastructure sites

Acknowledgements

The author would like to express our thanks to The National Research and Innovation Agency that has provided a scholarship through the doctoral degree by research program which has facilitated the implementation of this study at the Department of Civil Engineering, University of Indonesia. The author also acknowledges the assistance of Ms. Q.A. Khoirunnisa, undergraduate student of the Department of Geology, University of Indonesia, for her contribution to the cartographic refinement and graphical modification of Figures 1 and 2 based on the referenced earthquake source and geological datasets.

References

Abrahamson, N. A., 1992. Non-stationary spectral matching. *Seismological research letters*, 63 (1), p.1-30.

Abrahamson, N.A., Kamai, R., and Walter, J. S., 2013. Nonlinear Horizontal Site Response for the NGAWest2 Project: PEER Report 2013/12 Pacific Earthquake Engineering Research Center. *University of California, Berkeley.*

Al Atik, L. and Abrahamson, N., 2010. An improved method for nonstationary spectral matching. *Earthquake Spectra*, 26 (3), p.601-617.

Aribowo, S., Husson, L., Natawidjaja, D.H., Authemayou, C., Daryono, M.R., Puji, A.R., Valla, P.G., Pamumpuni, A., Wardhana, D.D., De Gelder, G., and Djarwadi, D., 2022. Active back-arc thrust in northwest Java, Indonesia. *Tectonics*, 41 (7), p.1-23. e2021TC007120

Bani-Hani, K. and M.A.I., 2017. A Multi-step approach to generate response-spectrum-compatible artificial earthquake accelerograms. *Soil Dynamics and Earthquake Engineering*, 97, p.117-32.

BAPETEN, 2013. *Seismic Aspect of Site Evaluation for Nuclear Installations*. *BCR No. 8.*

Barani, S., Ferretti, G., and Scafidi, D., 2022. A liquefaction triggering map for Italy. *MILQ:EGUsphere*, p.1-23.

Bardet, J. and Tobita, T., 1992. Soil liquefaction during earthquakes: recent advances and research directions. *Soil Dynamics and Earthquake Engineering*, 11 (6), p.303-333. doi:10.1016/0267-7261(92)90020-D.

BATAN, 2016. *Site Evaluation Report of RDE on Seismic Aspect*.

Bazzurro, P. and Cornell, C.A., 1999. Disaggregation of seismic hazard. *Bulletin of the Seismological Society of America, 89 (2)*, p.501-520.

Bazzurro, P. and Cornell, C.A., 2004. Ground-motion amplification in nonlinear soil sites with uncertain properties. *Bulletin of the Seismological Society of America*, 94 (6), p.2090-2109.

Bommer, J. and Acevedo, A., 2004. The use of real earthquake accelerograms as input to

dynamic analysis. *Journal of Earthquake Engineering,* 8 (spec01), p.43-91.

Bray, J.D., 2006. Assessment of the liquefaction susceptibility of fine-grained soils. *Journal of Geotechnical and Geoenvironmental Engineering*, 132 (9), p.1165-1177.

Cotton, F., Scherbaum, F., Bommer, J. J., and Bungum, H., 2006. Criteria for selecting and adjusting ground-motion models for specific target regions: Application to central Europe and rock sites. *Journal of Seismology*, 10 (2), p.137-156.

Damanik, R., Supendi, P., Widiyantoro, S., Rawlinson, N., Ardianto, A., Gunawan, E., Husni, Y.M., Zulfakriza, Z., Sahara, D.P., and Shiddiqi, H.A., 2021. Earthquake monitoring of the Baribis Fault near Jakarta, Indonesia, using borehole seismometers. *Geoscience Letters*, 8:38 (1), p.1-9. DOI:10.1186/s40562-021-00209-4

Dheeraj Vaidya, A.W., 2023. (n.d.). *Magnitude Frequency Distribution*. https://www.wallstreetmojo.com/frequency-distribution/. Retrieved from WallStreet- Mojo.

Dombi, J., Vranković Lacković, A., and Lerga, J., 2023. A New Insight into Entropy Based on the Fuzzy Operators,. Applied to Useful Information Extraction from Noisy Time-Frequency Distributions. *Mathematics*, 11 (3), p.1-23.

Drouet, S., Cotton, F., and Akkar, S., 2017. Seismic hazard disaggregation: a review of recent progress. *Bulletin of Earthquake Engineering*, 15 (7), p.2631-2665.

EERI Committee on Seismic Risk, 1989. The basics of seismic risk analysis. *Earthquake Spectra*, 5 (4), p.675-702.

Gonick, L., 1993. *The Cartoon Guide to Statistics.* Harper Perennial.

Goulet, C., Kishida, T., Ancheta, T., Cramer, C., Darragh, R., Silva, W., and Youngs, R., 2021. PEER NGA-east database. *Earthquake Spectra,* 37 (1_suppl), p.1331-1353.

Haifani, A.M. and Siwhan, N., 2022. The determination of earthquake sources contribution in the study of Seismic hazards for liquefaction of prospective sites for nuclear power plant, Bishkek, Kyrgyzstan. *In AIP Conference Proceedings,* 252, (1), p.100004. AIP Publishing LLC.

Hanifa, N., Wibowo, S. B., and Sukamto, M., 2014. Seismic hazard microzonation for Bandung area based on peak ground acceleration. *Journal of Earthquake Science and Technology,* 12 (1), p.25-35.

Hashash, Y. M., Kim, B., Stewart, J. P., Rathje, E. M., Harmon, J. A., Musgrove, M. I., and Silva, W. J., 2016. Relative differences between nonlinear and equivalent-linear 1-D site response analyses. *Earthquake Spectra,* 32 (3), p.1845-1865.

Hu, J., Zhang, R., Ren, L., Wu, F., and Cao, W., 2022. Research on automatic pattern recognition algorithm of micro-seismic waveform characteristics in mines. Yanshilixue Yu Gongcheng Xuebao/Chinese. *Journal of Rock Mechanics and Engineering*, 41 (2), p.346-361.

Idriss, I.M., 2008. *Soil liquefaction during earthquakes*.

Irfan, M., El-Emam, M., Khan, Z., and Abdalla, J., 2012. Local site effects on seismic ground response of Dubai-Sharjah metropolitan area. *In GeoCongress 2012: State of the Art and Practice in Geotechnical Engineering*, 1, p.869-1878.

Irsyam, M., Hutabarat, D., Asrurifak, M., Imran, I., Widiyantoro, S., Hendriyawan, D., and Iai, S., 2015. Development of seismic risk microzonation maps of Jakarta city. *Geotechnics for catastrophic flooding events*, p.35-47.

JMA, J.M., 2011. *Tohoku Earthquake Strong Motion Records.*

Kagawa, T., Irikura, K., and Nozu, A., 2012. Characteristics of long-period ground motions in the Tokyo Bay area during the 2011 Tohoku earthquake. *Earth, Planets and Space,* 64 (7), p.649-654.

Kim, B., Hashash, Y. M., Stewart, J. P., Rathje, E. M., Harmon, J. A., Musgrove, M. I., and Silva, W. J., 2016. Relative differences between nonlinear and equivalent-linear 1-D

site response analyses. *Earthquake Spectra*, 32 (3), p.1845-1865.

Kramer, S., 2020. *Geotechnical Earthquake Engineering*. USA: Prentice Hall.

Lilhanand, K. and Tseng, W.S., 1988. Development and application of realistic earthquake time histories compatible with multiple-damping design spectra. *Proceedings of the 9th WCEE*, 2, p.819-824.

Lilhanand, K. and Tseng, W.S., 1987. Generation of synthetic time histories compatible with multiple-damping design response spectra. *Transactions of the 9th International Conference on Structural Mechanics in Reactor Technology, Vol. K1.*

Liu, J., Mei, L., Ding, W., Xu, K., Yang, H., and Liu, Y., 2023. Asymmetric propagation mechanism of hydraulic fracture networks in continental reservoirs. *Bulletin*, *135 (3-4)*, p.678-688.

Mardani, A., Jusoh, A., Nor, K. M., Khalifah, Z., Zakwan, N., and Valipour, A., 2015. Multiple criteria decision-making techniques and their applications–a review of the literature from 2000 to 2014. *Economic Research-Ekonomska Istraživanja,* 28 (1), p.516-571.

Mase, L.Z., Tanapalungkorn, W., Likitlersuang, S., Ueda, K., and Tobita, T., 2022. Liquefaction analysis of Izumio sands under variation of ground motions during strong earthquake in Osaka. *Japan. Soils and Foundations*, 62 (5), 101218.

McGuire, R.K., Silva, W.J., and Costantino, C.J., 2002. *Technical basis for revision of regulatory guidance on design ground motions: development of hazard-and risk-consistent seismic spectra for two sites*.

McGuire, R., Cornell, C., and Toro, G., 2005. The case for using mean seismic hazard. *Earthquake Spectra*, 21 (3), p.879-886.

McGuire, R.K., 2016. *Seismic hazard and risk analysis.*

Mergos, P. and Sextos, A., 2019. Selection of earthquake ground motions for multiple objectives using genetic algorithms. *Engineering Structures*, 187, p.414-427.

Miller, T., 2015. *Statistics. MAT*. College Mathematics.

Pagani, M., Monelli, D., Weatherill, G.A., and Garcia, J., 2014. *The OpenQuake-engine Book: Hazard. Global Earthquake Model (GEM)*.

Pitarka, A., Graves, R., Irikura, K., Miyakoshi, K., and Rodgers, A., 2020. A. Kinematic rupture modeling of ground motion from the M7 Kumamoto, Japan earthquake. *Pure and Applied Geophysics*, 177, p.2199-2221.

Silva, W.J. and Derras, B., 2019. Evaluation of the uncertainties and limitations of seismic hazard and risk assessments. *Natural Hazards and Earth System Sciences*, *19 (11)*, p. 2503-2520.

Supendi, P., Widiyantoro, S., Rawlinson, N., Daryono, M.R., Ardianto, A., Baskara, A.W., Damanik, R., and Husni, Y.M, 2025. Evidence of the West Java backarc thrust from earthquake activity. *Tectonophysics*, 230853.

Spassiani, I., Yaghmaei-Sabegh, S., Console, R., Falcone, G., and Murru, M., 2023. Comparison analysis of the ETAS model with Gutenberg–Richter (GR), Tapered-GR and characteristic magnitude distributions. *Geophysical International Journal*, 232 (1), p.413-428.

Stewart, J.P., Seyhan, E., and Boore, D.M., 2014. Nonlinear site amplification and its application in NGA-West2. *Earthquake Spectra, 30 (3)*, p.1285-1317. DOI:10.1193/063013eqs181m.

Widiyantoro, S., Supendi., P., Ardianto, A., Baskara, A.W., Bacon, C.A., Damanik., R., Rawlinson, N., Gunawan, E., Sahara, D. P., Zulfakriza, Z., Husni, Y. M., and Lesmana, A., 2022. Implications for fault locking south of Jakarta from an investigation of seismic activity along the Baribis fault, northwestern Java, Indonesia. *Scientific Report*, 12 (1), 10143, Doi:10.1038/s41598-022-13896-6

Wirth, E., Vidale, J.E., Frankel, A.D., Pratt, T L., Marafi, N.A., Thompson, M., and Stephenson, W.J., 2019. Source-dependent amplification of earthquake ground motions in deep sedimentary basins. *Geophysical Research Letters,* 46 (12), p.6443-6450.

Yassin, I.A., Patrisina, R., and Amrina, E., 2022. Location-Allocation Model for Victims and Health Workers during Post Earthquake-Tsunami Health Crisis in Padang City. *EV-ERGREEN Joint Journal of Novel Carbon Resource Sciences & Green Asia Strategy*, 09 (01), p.234-245.

Zafarani, H., Luzi, L., Lanzano, G., and Soghrat, M., 2018. Empirical equations for the prediction of PGA and pseudo spectral accelerations using Iranian strong-motion data. *Journal of Seismology,* 22, p.263-285.

Zimmerman, R.B., Baker, J.W., Hooper, J.D., Bono, S., Haselton, C.B., Engel, A., and Jalalian, A., 2017. Response history analysis for the design of new buildings in the NEHRP provisions and ASCE/SEI 7 standard: Part III-Example applications illustrating the recommended methodology. *Earthquake Spectra,* 33 (2), p.419-447.